JOURNAL OF OPTOELECTRONICS AND ADVANCED MATERIALS, Vol. 11, No. 12, December 2009, p. 2088 - 2092

X-ray diffraction analysis of PbTe/SnTe superlattices grown on Si(111) substrates

O. SHAPOVAL[a], A. BELENCHUK[a], A. FEDOROV[b], V. KANTSER[a], E. ZASAVITSKY[a*]
[a]*Institute of Electronic Engineering and Industrial Technologies, ASM, 3/3 Acdemiei str., 2028 Chisinau, Moldova*
[b]*Institute of Single Crystal, NASU, 60 Lenin ave., 61001 Kharkov, Ukraine*

The 50 period PbTe/SnTe superlattices (SLs) were grown on Si (111) substrates by hot-wall beam epitaxy (HWBE) using an intermediate fluoride buffer. The SL period varied from 6.6 to 24.0 nm with PbTe:SnTe thickness ratios of 2:1 and 1:1. The structural analysis was performed by X-ray diffraction and reflection measurement techniques. The resolution up to 8 orders of SL satellite diffraction peaks indicates well-formed SLs with sharp interfaces and long range ordering. The processing of X-ray spectra on the basis of dynamical theory of diffraction was used for estimation of individual layer thicknesses and residual strains. The differences in lattice parameters both between SL components and relative to the substrate, as well as the thermal expansion coefficient mismatch of A^4B^6 compounds with regard to the substrate, are the reasons for the strains appearing in this SL structure. Fitted parameters of the normal lattice mismatch revealed that the SnTe layers are equally strained independent of thickness, whereas the stress of PbTe layers is progressively decreasing with thickness. In spite of residual lattice mismatch strain, the SL structures exhibited ability to full relax of the thermal mismatch strains as in the case of earlier investigated single layers of A^4B^6 grown on Si (111) coated with fluoride buffer. Our results indicate the possibility to fabricate high efficient thermoelectric coolers based on PbTe/SnTe SLs directly integrated with Si chips.

(Received July 5, 2009; accepted November 12, 2009)

Keywords: PbTe, SnTe, Superlattice, Si substrate, Fluoride buffer, X-ray diffraction, Simulation, Strain relaxation

1. Introduction

The crystalline parameters of the A^4B^6 narrow gap semiconductor SLs were studied in a number of works [1-3]. Main attention was paid to their optoelectronic applications as IR lasers and detectors. The systems based on solid solutions were in greater demand due to low lattice parameter mismatch and, therefore, to higher crystalline perfection of SLs. The investigations were focused mainly on the growth of the SLs on a bulk BaF_2 (111) crystal substrate that is the best matched compound to A^4B^6 semiconductors by lattice parameter and thermal expansion coefficient.

The renewal of interest to A^4B^6 based SLs was invoked by their considerable potential for the thermoelectricity applications. The enhancement in the figures-of-merit ZT ($ZT=S^2\sigma/\kappa$; S –Seebeck coefficient, σ and κ electrical and thermal conductivities, respectively) for SLs was obtained by reduction of the thermal conductivity κ across layers with simultaneous preservation the high electrical conductivity σ. For such phonon-blocking/electron-transmitting structures, the highest value of ZT=2.4 was achieved in the short-period Bi_2Te_3/Sb_2Te_3 SLs [4]. The A^4B^6 semiconductor SLs have some advantages over Bi_2Te_3-based ones in crystalline quality of obtained SLs [5] and, therefore, they are preferable for further fabrication of more efficient thermoelectric devices. For this purpose, the PbTe/SnTe SLs reveals an advantage compared to the earlier investigated PbTe/PbSe SL system due to more difference in phonon spectra [6,7], which is important for suppression of the lattice thermal conductivity in cross direction of SL. Another important reason in favor to the A^4B^6-based SLs in comparison with Bi_2Te_3-based is connected with their unique ability of a monolithic integration with Si chips. The hybrid technology used now for integration of thermoelectric coolers fabricated of Bi_2Te_3-based SLs does not provide high efficient thermal conductivity interface with Si chip [8]. On the other hand, the SLs based on A^4B^6 semiconductor can be epitaxially integrated with Si chips. Despite the high difference of the thermal expansion coefficient between A^4B^4 semiconductors and Si substrate, the epitaxial growth is possible by using the BaF_2/CaF_2 buffer layer [9].

To our knowledge, there was the only work concerned with detailed investigation of PbTe/SnTe SLs grown on BaF_2 (111) substrate [10] and there are no investigations focused on SLs grown on more practically important Si substrates. In this work, we present the results of the structural investigations of the PbTe/SnTe SLs grown epitaxially on Si (111) substrate coated with epitaxial fluoride buffer. The high lattice mismatches between the SL components and substrate may cause the crystalline quality degradation. This problem can be partially solved by introducing of the relatively thick PbTe buffer layer with high structural quality used as fully strain free substrate for the SLs. Another problem is related with a very high difference of the thermal expansion coefficients between A^4B^6 semiconductors based SL and Si substrate. A question of principle is to what extent the well known mechanism of the thermal strain relaxation by dislocation glide in the main glide system of the A^4B^6 semiconductors

[11] allows us to restore structural perfection of the epitaxial SL on the Si substrate.

2. Experimental

In this work, Si (111) wafers were used as an initial substrate. The substrate preparation for SL growth was performed in two stages. At first step, a stacked epitaxial buffer layer BaF_2/CaF_2 was deposited on Si (111) wafer in MBE system after standard substrate cleaning procedure [12]. At second step, the structure of BaF_2/CaF_2/Si (111) was transferred into HWBE deposition system equipped with PbTe and SnTe cells and additional Te_2 sources at each cell. After preheating of the substrate at 420°C, the PbTe buffer layer growth was performed typically at 360°C. Then, the growth of the SL structures was carried out at the same technological process just after deposition of the ~4 μm thick PbTe buffer layer. For the SL deposition, the substrate temperature was decreased down to 270°C in order to eliminate interdiffusion process at heterointerfaces between PbTe and SnTe layers and to ensure abrupt interfaces. The growth rate was about 0.35-0.42 nm/s (close to 1 ML/s) for both materials.

Two types of PbTe/SnTe SLs have been grown. The first type has the individual layer thickness ratio between PbTe and SnTe of 2:1; the second one, 1:1. Number of repetition was 50 for all grown SLs and the period ranged from 6.5 to 24.0 nm. For all SLs, the thickness of SnTe layers was still well below the critical thickness of epitaxy on PbTe that is around 10.0 nm [13]. The critical thickness of the whole SL grown on the top of PbTe buffer can be evaluated from the simple relation $T_c=1/f$ (in monolayers) [14], where f is the misfit between average SL lattice parameter and PbTe one. The calculated critical thicknesses of the whole PbTe/SnTe SL relative to PbTe are 53 and 36 nm for the value of the individual layer ratios of 2:1 and 1:1, respectively. Therefore, the number of repetitions was large enough and, as a whole, even the thinnest SLs are expected to be relaxed relative to the PbTe buffer.

The surfaces of the PbTe and BaF_2/CaF_2 buffer layers were investigated by STM and AFM, respectively. The X-ray diffraction (XRD) and reflection (XRR) analysis was performed by means of a double-crystal spectrometer using Cu $K_{\alpha 1}$ radiation. It was found that, with the accuracy of measurement, the position of (111) peak from thick PbTe-buffer is well matched to the one taken from bulk PbTe. However, the peak (111) of the BaF_2 buffer layer was slightly shifted from the bulk crystal position, which indicates small residual tension of the BaF_2 lattice in the surface plane. Therefore, the position of PbTe (111) peak was used as a reference mark to determination of the SL satellite positions. The (111) diffraction peaks from SLs measured experimentally were compared with simulated ones. The simulation of dynamical X-ray diffraction from SL structures was carried out using the Rocking Curve Simulation program, whereas the data of the crystal susceptibilities X0, Xh for PbTe and SnTe were calculated by the X0hWin program [15].

3. Results and discussion

3.1. Surface of buffer layers

Typical BaF_2/CaF_2 buffer layer was 180/3 nm thick and the root mean square (RMS) of surface roughness tested by AFM was about 0.5-0.7 nm as shown in Fig. 1(a). Buffer PbTe layers grown at 360°C had good crystalline quality and surface morphology. For 4 μm thick PbTe layer FWHM rocking curve of the diffraction (333) line was 90-130 arcsec and RMS of the surface roughness was about 10-15 Å as shown in Fig. 1(b). The three sets of straight lines in both surface images are directed parallel to three ⟨011⟩ surface directions, the intercepts of the {100} planes with the surface. These one- or two-monolayer steps result from the thermal strain relaxation mechanism by dislocation glide in the {100} planes during cool down from growth to room temperature [11].

3.2. X-ray diffraction measurements

Figure 2 shows three θ-2θ X-ray diffraction spectra measured around the (111) Bragg peak for the set of the PbTe/SnTe SLs with the periods related as 1:2:3. The evidence for a SL formation is confirmed by well-formed satellite peaks up to 8th order. The zero-order peak SL0 of the structure appears as the most intense peak among the satellites and locates on the higher angle side near the PbTe buffer peak. Therefore, the average out-of-plane lattice parameter of the SL is smaller than that of the PbTe buffer. The satellite peaks are well scaled in accordance to relation between periods of presented SLs. Since on our samples the PbTe/SnTe SL and PbTe buffer did not cover all surface of the BaF_2/CaF_2/Si(111) substrate, the (111) BaF_2 diffraction peaks originated from free surface of the BaF_2 buffer layer.

3.3. SL period determination

The SL period T can by accurately determined from the equation [16]

$$(2\sin\theta_n - 2\sin\theta_{SL}) = \pm n\lambda/T \quad (1)$$

where λ is the X-ray wavelength, n is the order of satellite peaks, θ_n is the diffraction angle of the satellite peak, and θ_{SL} is the Bragg angle of the host lattice. For some samples, the SL periods obtained from high angle XRD were compared with data calculated from low angle XRR. For the calculation of the SLs period from small angle XRR, we used the method described in [17]. The SL period can be calculated from the angular position of the satellites peak θ_n. Since the X-ray beam is applied to the sample at small incident angle, the effect of X-ray refraction at the surface and the interface must be considered. The modified Bragg low is given by

$$d = [1-(1-n_{SL})/\sin^2\theta_n] \quad (2)$$

where $d=n\lambda/2\sin\theta_n$, and n_{SL} is the average X-ray refractive index of the SL. Fig. 3 shows the XRR spectrum and the plot of d *vs* $1/\sin^2\theta_n$. As is expected from the equation (2), the just straight line is obtained. The SL period T was determined from the crossing point of the extrapolated straight line with the d axes. Data of the PbTe/SnTe SL samples obtained from the X-ray analysis by XRR and XRD are well-matched and shown in Table.

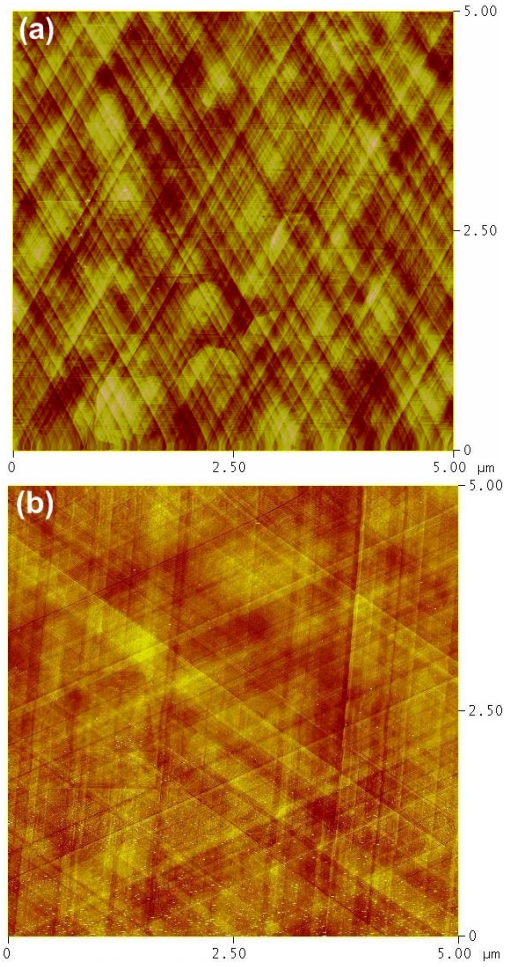

Fig.1. Surface morphology of buffer layers: (a) AFM image of 180 nm thick BaF_2 buffer with RMS of roughness of 0.59 nm and (b) STM image of 4 μm thick PbTe buffer with RMS of roughness of 1.2 nm.

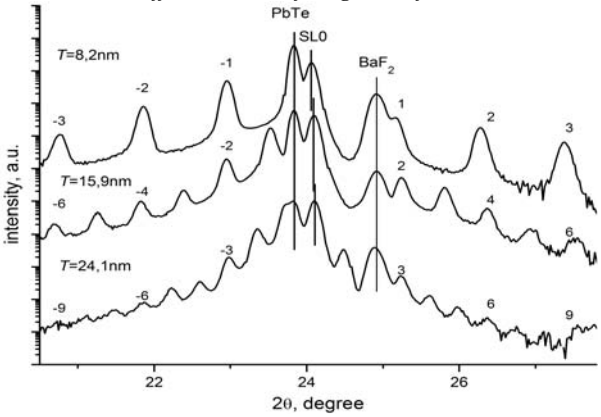

Fig.2. Experimental X-ray diffraction spectra of the PbTe/SnTe SLs with periods 8.2, 15.9, and 24.1 nm grown on PbTe/BaF_2/CaF_2/Si(111) substrates.

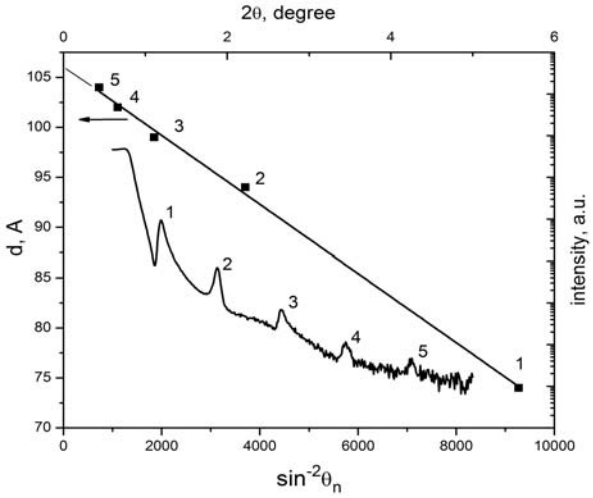

Fig.3. The small angle X-ray reflection pattern and the plot of $d=n\lambda/2\sin\theta_n$ vs $1/\sin^2\theta_n$ for PbTe/SnTe SL. The intercept of the extrapolated line along the d axis shows the SL period.

Table. Data of the PbTe/SnTe SL samples obtained from the X-ray analysis.

sample	period T, nm		simulation				
	small angle XRR	XRD (111) reflection	period, nm	PbTe		SnTe	
				thickness, nm	normal lattice mismatch Δa/a	thickness, nm	normal lattice mismatch Δa/a
06		24.1±0.14	24.1	16.4	$1\cdot10^{-3}$	7.7	$-3.4\cdot10^{-2}$
07	15.93±0.07	15.82±0.09	15.9	10.9	$1.5\cdot10^{-3}$	5.0	$-3.3\cdot10^{-2}$
08		8.13±0.09	8.2	5.6	$3\cdot10^{-3}$	2.6	$-3.3\cdot10^{-2}$
12	6.53±0.02	6.62±0.37	6.7	3.6	$6\cdot10^{-3}$	3.1	$-3.4\cdot10^{-2}$

15	10.61±0.04	10.83±0.07	10.8	5.9	$3.5\cdot10^{-3}$	4.9	$-3.4\cdot10^{-2}$

3.4. X-ray diffraction simulation

The fitting parameters for the processing of the diffraction curves were chosen from the following considerations. The Poisson ratio for cubic lattice with (111) orientation can be found [18] using the expression

$$\gamma_{111} - \frac{1}{2}\frac{C_{11} + 2C_{12} - 2C_{44}}{C_{11} + 2C_{12} + C_{44}} \quad (3)$$

where the elastic constants in GPa used for PbTe were C_{11}=108, C_{12}=7.7, C_{44}=13.4 and C_{11}=109, C_{12}=2.1, C_{44}=9.7 for SnTe [19]. The data of surface roughness of the PbTe buffer layer were established from STM measurement, and for individual layers it was considered of about 1 ML as assessed value. To obtain better matching to experimental curve we varied the both parameter: the individual layer thickness and the normal lattice spacing mismatch $\Delta a/a$. The $\Delta a/a$ value reflect the strain of the lattice parameter in the ⟨111⟩ direction. Reasonable values of the individual thicknesses were fitted due to the set of the experimental diffraction patterns from SL with periods related as 1:2:3 and the presence of the missing peak +SL1 on one of the spectra (Fig. 4). As one can see from Fig. 2, distance between zero peak position of the SL and PbTe buffer layer increases with increasing of the SL period. Adjustments of the normal lattice mismatch parameter allow us to conclude that the PbTe layers are strained. The degree of the strain relaxation in the PbTe layers increases with the increment of their thickness that results in a shift of the zero peak SL position more and more farther from PbTe buffer peak. The strain in the PbTe component of the SL structure decreased as the PbTe thickness increased from 3.6 to 16.4 nm (Table). At the same time, the SnTe layers suffer significant strain and became deformed elastically for all used thicknesses.

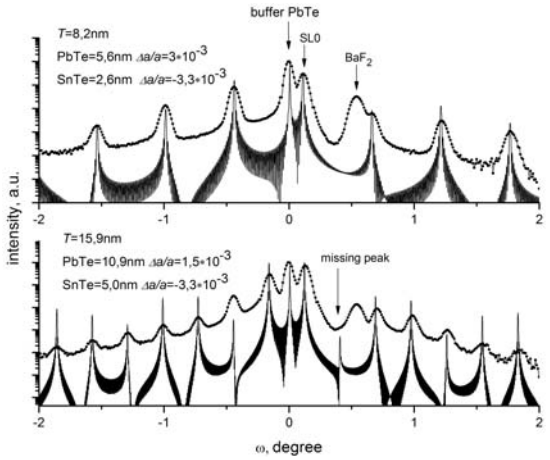

Fig.4. X-ray experimental data and simulations of the (111) ω-2θ scan for two SL PbTe/SnTe. The SLs exhibit different normal lattice strain Δa/a for PbTe individual layers.

The best fit was achieved with the variation of period around the mean value about 2% for SL with a period of 8.2 nm (Fig. 3). The pseudomorphic first repetition and the fully oxidized last one were taken into account. We have also assumed that there is no significant strain gradient through structure. More complex character of the individual layer perfection parameter for a thicker SL allows us to determine the only combination of the individual layer thickness and the $\Delta a/a$ parameter, at which the missing peak was observed.

We suppose that the growth PbTe/SnTe SL was accompanied with the growth process described in [10, 20]. The PbTe and SnTe layers grow one upon the other in a layer-by-layer mode with the formation of misfit dislocations at the thicknesses more than d=2 nm. Each successive epitaxial layer inherits all threading dislocations from the preceding epitaxial layer. The reduction of structural perfection of the SL layers in our simulations was taken into account by gradually modified static Debye-Waller factor [21]. The relatively thin (<10 nm) SnTe layers remain elastically deformed under significant stress. Grown SL structures occupy the intermediate position relative to fully pseudomorphic and fully relaxed structures. Grown structures belong to non-pseudomorphic and non-coherent SL according to our estimation. The in-plane lattice parameters of the SL components are smaller than for PbTe buffer layer and non-coincident with each other.

3.5. Thermal strain relaxation

The strain conditions for SLs grown on Si (111) substrate differ considerably from those for SLs grown on bulk BaF_2(111) crystal. Additional strain arises in the whole structure after growth, during the cooling process, due to the difference of the thermal expansion coefficient between Si substrate and A^4B^6 semiconductors. To withstand the thermal strain, the SL has to relax simultaneously with the PbTe buffer despite multi-interface structure of SL with lattice parameters alternated both in-plane and out-of-plane directions.

To estimate the ability for thermal strain relaxation, the thermal cycles between RT and 77 K were applied by direct dipping of samples into liquid nitrogen and warming them rapidly back to room temperature. X-ray diffraction measurements were carried out before and after such thermocycling. No appreciable reducing of the intensity and broadening of the diffraction peaks was detected on the tested structures even after several cycles. This indicates to the absence of the significant degradation of the crystalline quality of the SLs due to great thermal coefficient mismatch with Si substrate. Despite of a complex structure consisted of a great number of different interfaces; the crystalline quality of layers and interfaces provides the glide of dislocations across the whole of

epitaxial system according to the well-known mechanism of strain relaxation [11].

4. Conclusions

In summary, we have prepared a series of PbTe/SnTe superlattices using the approach of complex epitaxially stacked PbTe/BaF_2/CaF_2 buffer on Si (111) substrates. The growth conditions induced strains in the PbTe/SnTe SLs in different mode for PbTe and SnTe components. The SnTe layers with thicknesses 2.6-7.7 nm preserve strained state closely to pseudomorphic one independent of thickness. The degree of their strain relaxation is low relative to PbTe buffer. Alternatively, the PbTe layers relax the stress progressively with increasing of their thickness from 3.6 to 16.4 nm. At the same time, SL exhibits an excellent ability of thermal mismatch strain relaxation. The epitaxial A^4B^6 structures consisting of PbTe/SnTe SLs and PbTe buffers relax stress completely despite the great number of periods and heavy thermal coefficient mismatch with Si substrate. The technology of epitaxial growth of PbTe/SnTe SLs on Si substrates can be further used for fabrication of thermoelectrical coolers monolithically integrated with Si chips.

References

[1] M.Kriechbaum, K.E.Ambrosch, E.J.Fantner, H.Clements, G.Bauer, Phys. Rev. B **30,** 3394 (1984).
[2] G. Springholz,Molecular Beam Epitaxy of IV-VI Heterostructures and Superlattices, in: Lead Chalcogenides: Physics and Applications, Taylor and Francis, Philadelphia, 2002, p.123.
[3] E.Abramof, P.H.O.Rapple, A.Y.Ueta, P.Motisuke, J. Appl. Phys. **88**, 725 (2000).
[4] R. Venkatasubramanian, E. Silvola, T. Colpitts, Nature **413**, 597 (2001).
[5] J. C. Caylor, K. Coonley, J. Stuart, T. Colpitts, and R. Venkatasubramanian, Appl. Phys. Lett. **87**, 023105 (2005).
[6] David G. Cahill, Wayne K. Ford, Kenneth E. Goodson, Gerald D. Mahan, Arun Majumdar, Humphrey J. Maris, Roberto Merlin, Simon R. Phillpot, J. Appl. Phys. **93**, 793 (2003).
[7] Nabonita D. Chowdhury, Sankar P. Sanyal, Pramana-J. Phys. **43**, 397 (1994).
[8] Ihtesham Chowdhury, Ravi Prasher, Kelly Lofgreen, Gregory Chrysler, Sridhar Narasimhan, Ravi Mahajan, David Koester, Randall Alley, Rama Venkatasubramanian, Nature Nanotechnology **4**, 235 (2009).
[9] H. Zogg, C. Maissen, J. Masek, T. Hoshino, S. Blunier, and A. N. Tiwari, Semicond. Sci. Technol. **6**, C36 (1991).
[10] S. O. Ferreira, E. Abramof, P. H. 0. Rappl, A. Y. Ueta, H. Closs, C. Boschetti, P. Motisuke, I. N. Bandeira, J. Appl. Phys. **84**, 3650 (1998).
[11] H. Zogg, S. Blunier, A. Fach, C. Maissen, P. Müller, S. Teodoropol, V. Meyer, G. Kostorz, A. Dommann, T. Richmond, Phys. Rev. B **50**, 10801 (1994).
[12] A.Belenchuk, O.Shapoval, V.Kantser, A.Fedorov, P.Schunk, Th.Schimmel, Z.Dashevsky, J. Crys. Growth **198/199**, 1216 (1999).
[13] A.I.Fedorenko, O.N.Nashchekina, B.A.Savitskii, L.P.Shpakovskaya, Vacuum **43**, 1191 (1992).
[14] D. J. Dunstan, S. Young, and R. H. Dixon, J. Appl. Phys. **70**, 3038 (1991)
[15] S.Stepanov, Proceedings SPIE, **5536**, 16 (2004).
[16] P.F.Fewster, Superlattices, in: X-Ray and Neutron Dynamical Diffraction, Plenum Press, New York,1996, p.286.
[17] M.Sugawara, M.Kondo, S.Yamazaki, K.Nakajima, Appl. Phys. Lett. **52**, 742 (1988).
[18] M.A.Meram, M.E.Vickers, Rep. Prog. Phys. **72**, 036502 (2009).
[19] G.Nimtz, Numerical data and Functional Relationship in Science and Technology. New Series Group III 17 (1993) 146.
[20] E.I. Rogacheva, S.N. Grigorov, O.N. Nashchekina, T.V. Tavrina, S.G. Lyubchenko, A.Yu. Sipatov, V.V. Volobuev, A.G. Fedorov, M.S. Dresselhaus, Thin Solid Films **493**, 41 (2005).
[21] A.G.Krasilnikov, V.I.Punegov, N.N.Faleev, Pisma JTF **30**, 6 (2004).

*Corresponding author: efim@hises.asm.md